Comparison of Two Model Frameworks for Fiber Dispersion in the Elasticity of Soft Biological Tissues*

Gerhard A. Holzapfel[1,2] and Ray W. Ogden[3]

[1]Institute of Biomechanics, Graz University of Technology
Stremayrgasse 16-II, 8010 Graz, Austria

[2]Norwegian University of Science and Technology (NTNU)
Faculty of Engineering Science and Technology, 7491 Trondheim, Norway

[3]School of Mathematics and Statistics, University of Glasgow
University Place, Glasgow G12 8SQ, Scotland, UK

Revision submitted to ***Eur. J. Mech. A/Solids***
July 6, 2017

Abstract. This study compares two models that are used to describe the elastic properties of fiber-reinforced materials with dispersed fibers, in particular some soft biological tissues such as arterial walls and cartilages. The two model approaches involve different constitutive frameworks, one being based on a generalized structure tensor (GST) and the other on the method of angular integration (AI). By using two representative examples, with the same number of parameters for each model, it is shown that the predictions of the two models are virtually identical for a significant range of large deformations, which contradicts conclusions contained in several papers that are based on faulty analysis. Additionally, each of the models is fitted to sets of uniaxial data from the circumferential and axial directions of the adventitia of a human aorta, both models providing excellent agreement with the data. While the predictions of the two models are comparable and exclusion of compressed fibers can be accommodated by either model, it is well known that the AI model requires more computational time than the GST model when used within a finite element environment, in particular if compressed fibers are excluded.

Keywords: Fiber dispersion model; generalized structure tensor; angular integration model; fibrous tissue

1 Introduction

Collagen fibers are ubiquitous load-bearing and reinforcing elements in fibrous tissues and are thus important from both structural and mechanical perspectives. Experimental data confirm

*Based in part on the Rodney Hill Prize Lecture presented by Ray W. Ogden at the 24$^{\text{th}}$ International Congress of Theoretical and Applied Mechanics, Montréal, Canada, August 24, 2016.

that the arrangement of collagen fibers is in general highly dispersed, depending on, e.g., the type of tissue, such as for human arterial tissues [1, 2] and articular cartilage [3, 4]. In addition, the collagen fiber arrangement also changes with disease such as in the abdominal aorta [5] and the myocardium [6, 7]. Structural quantifications of the collagen fabric can be identified by a variety of imaging methods such as polarized light microscopy [1], synchrotron X-ray diffraction [8], second-harmonic generation [2] and ultra-high field diffusion tensor magnetic resonance imaging [9], *inter alia*. These approaches allow a detailed geometrical reconstruction of the micro-architecture, which serves as a basis for continuum mechanical modeling and computational analysis. Continuum models that accommodate fiber dispersion within a non-collagenous matrix have been developed in recent years with particular reference to the elastic response of arteries [10, 11] and the myocardium [12], but have also been used for heart valves [13], corneas [14], articular cartilage [9], etc.

There are two main approaches for modeling fiber dispersion in the context of the mechanics of soft biological tissues, namely the 'angular integration' (AI) and 'generalized structure tensor' (GST) approaches. In order to describe and compare these we make use of the deformation gradient $\mathbf{F}$, the right Cauchy–Green tensor $\mathbf{C} = \mathbf{F}^{\mathrm{T}}\mathbf{F}$, and the stretch $\lambda = \sqrt{\mathbf{N} \cdot \mathbf{C}\mathbf{N}}$ in the direction of the unit vector $\mathbf{N}$ in the reference configuration corresponding to the direction of the orientation of an arbitrary individual fiber.

The AI approach was formulated by Lanir [15]. In this approach, an individual fiber within a dispersion is considered to have a strain energy $w(\lambda)$, with the properties $w(1) = w'(1) = 0$ in the reference configuration assuming that there is no residual stress. Whereas in [15] the possibility of w being different for different fibers was considered, here, for simplicity, we assume that w is the same for each of the fibers. Supposing that there are n such fibers per unit reference volume which are dispersed according to the angular density distribution $\rho(\mathbf{N})$, with $\rho(-\mathbf{N}) = \rho(\mathbf{N})$, the strain-energy function Ψ_{AI} of the combined fibers and matrix per unit reference volume is given by

$$\Psi_{\mathrm{AI}} = n \int_{\Omega} \rho(\mathbf{N}) w(\lambda) \mathrm{d}\Omega + \Psi_{\mathrm{iso}}, \tag{1}$$

where Ψ_{iso} refers to the energy stored in the non-collagenous matrix material in which the fibers are embedded. The contribution Ψ_{iso}, which is normally assumed to be isotropic, was not included by Lanir [15]. It is assumed that Ψ_{AI} vanishes in the reference configuration and is not associated with any residual stress. In addition, Ω is the unit sphere, and ρ is normalized according to

$$\frac{1}{4\pi} \int_{\Omega} \rho(\mathbf{N}) \mathrm{d}\Omega = 1. \tag{2}$$

The GST approach, formulated by Gasser et al. [10], is based on a so-called generalized structure tensor defined by

$$\mathbf{H} = \frac{1}{4\pi} \int_{\Omega} \rho(\mathbf{N}) \mathbf{N} \otimes \mathbf{N} \mathrm{d}\Omega, \tag{3}$$

which is the mean of the individual structure tensors $\mathbf{N} \otimes \mathbf{N}$ of the fibers in the dispersion weighted by the orientation density ρ. From the normalization (2) it follows that $\mathrm{tr}\mathbf{H} = 1$. In this approach the energy function per unit reference volume associated with the fibers is denoted by Ψ_{f} with the condition $\Psi_{\mathrm{f}}(\mathbf{I}, \mathbf{H}) = 0$, where $\mathbf{I}$ is the identity tensor, and it is also assumed that it is not associated with any residual stress. The total energy function including that of the matrix is then

$$\Psi_{\mathrm{GST}} = \Psi_{\mathrm{f}}(\mathbf{C}, \mathbf{H}) + \Psi_{\mathrm{iso}}. \tag{4}$$

It should be emphasized that Ψ_{AI} and Ψ_{GST} are in general completely different functions. For a summary of models based on these two approaches, see the introduction in [11].

In other studies we have also introduced modifications of both the AI and GST models that exclude the contributions of compressed fibers [16–19], and we refer to these works for detailed discussion. We note, however, that for either model, depending on the considered deformation, exclusion of compressed fibers can have a significant effect on the material response, but, for purposes of comparison here these modifications are not needed. It should be pointed out that previous comparisons of the AI and GST models in the literature have been based on incorrect arguments; see, e.g., [20], repeated in [21–24] and other studies, as recently discussed in [17]. The main purpose of the present paper is therefore to show that the predictive powers of the two models are virtually identical for a significant range of large deformations, in contrast of the conclusions in [20–24] .

2 The Cauchy stress tensors of the AI and GST models

For further development of the energy functions and the related stresses we now define a number of invariants associated with the kinematics. In general, since the matrix is considered to be isotropic, Ψ_{iso} depends on the isotropic invariants

$$I_1 = \mathrm{tr}\mathbf{C}, \quad I_2 = \frac{1}{2}(I_1^2 - \mathrm{tr}\mathbf{C}^2), \quad I_3 = \det \mathbf{C}. \tag{5}$$

For incompressible isotropic materials $I_3 = 1$ and the energy function Ψ_{iso} depends only on I_1 and I_2, but for incompressible soft tissues, on which we focus here, Ψ_{iso} is normally treated as a

function of I_1 alone. Associated with the fiber direction $\mathbf{N}$ there are two invariants that combine $\mathbf{C}$ and $\mathbf{N} \otimes \mathbf{N}$. These are denoted by $I_4(\mathbf{N})$ and $I_5(\mathbf{N})$ and defined by

$$I_4(\mathbf{N}) = \mathbf{N} \cdot \mathbf{CN} = \mathbf{n} \cdot \mathbf{n}, \quad I_5(\mathbf{N}) = \mathbf{N} \cdot \mathbf{C}^2\mathbf{N} = \mathbf{n} \cdot \mathbf{Bn}, \tag{6}$$

where $I_4(\mathbf{N}) = \lambda^2$, $\mathbf{n} = \mathbf{FN}$, which is the push forward of $\mathbf{N}$ under the deformation, and $\mathbf{B} = \mathbf{F}\mathbf{F}^{\mathrm{T}}$ is the left Cauchy–Green tensor. In addition, we introduce the generalized invariants, denoted $I_4^\star$, $I_5^\star$, as

$$I_4^\star = \mathrm{tr}(\mathbf{HC}), \quad I_5^\star = \mathrm{tr}(\mathbf{HC}^2). \tag{7}$$

The Cauchy stress tensor $\boldsymbol{\sigma}$ for a general energy function Ψ for an incompressible material is given by

$$\boldsymbol{\sigma} = 2\mathbf{F}\frac{\partial \Psi}{\partial \mathbf{C}}\mathbf{F}^{\mathrm{T}} - p\mathbf{I}, \tag{8}$$

where p is a Lagrange multiplier. Then, by taking $\Psi = \Psi_{\mathrm{AI}}$ and $\Psi = \Psi_{\mathrm{GST}}$ from eqs. (1) and (4), respectively, we obtain

$$\boldsymbol{\sigma}_{\mathrm{AI}} = n\int_\Omega \rho(\mathbf{N})\lambda^{-1}w'(\lambda)\mathbf{n} \otimes \mathbf{n}\mathrm{d}\Omega + \boldsymbol{\sigma}_{\mathrm{iso}} - p\mathbf{I}, \tag{9}$$

$$\boldsymbol{\sigma}_{\mathrm{GST}} = 2\mathbf{F}\frac{\partial \Psi_{\mathrm{f}}(\mathbf{C}, \mathbf{H})}{\partial \mathbf{C}}\mathbf{F}^{\mathrm{T}} + \boldsymbol{\sigma}_{\mathrm{iso}} - p\mathbf{I}, \tag{10}$$

where $w' = \mathrm{d}w/\mathrm{d}\lambda$, and $\boldsymbol{\sigma}_{\mathrm{iso}} = 2\psi_{\mathrm{iso}\,1}\mathbf{B} + 2\psi_{\mathrm{iso}\,2}(I_1\mathbf{B} - \mathbf{B}^2)$ is the contribution of Ψ_{iso} to the isotropic stress in the matrix material, with $\psi_{\mathrm{iso}\,i} = \partial\Psi_{\mathrm{iso}}/\partial I_i$, $i = 1, 2$, but $\psi_{\mathrm{iso}\,2}$ is taken to be zero in the present context. For detailed reference to the relevant background from continuum mechanics, see the textbooks [25, 26].

3 Rotationally symmetric dispersion

For simplicity we now assume a rotationally symmetric dispersion for which the mean fiber direction is the unit vector $\mathbf{M}$. We use the notation $\mathbf{m}$ for its image $\mathbf{FM}$ in the deformed configuration, and note that $\mathbf{m}$ is not, in general, the mean fiber direction in the deformed configuration, nor is it a unit vector. The generalized structure tensor in this case reduces to

$$\mathbf{H} = \kappa\mathbf{I} + (1 - 3\kappa)\mathbf{M} \otimes \mathbf{M}, \tag{11}$$

where the constant κ is referred to as a dispersion parameter and is defined by [10]

$$\kappa = \frac{1}{4}\int_0^\pi \rho(\Theta)\sin^3\Theta\mathrm{d}\Theta, \tag{12}$$

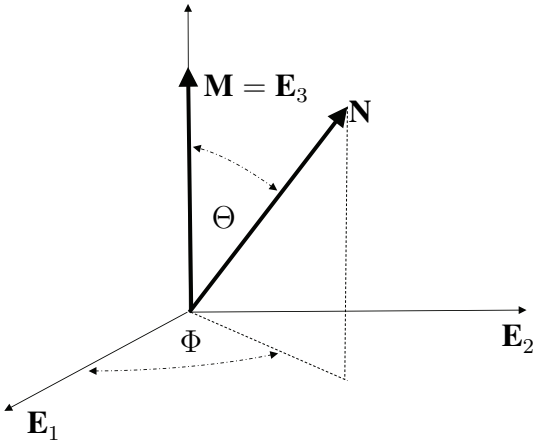

Figure 1: The direction **N** of an arbitrary fiber within a rotationally symmetric dispersion with mean fiber direction $\mathbf{M} = \mathbf{E}_3$. The fiber is referred to rectangular Cartesian coordinates with basis vectors $\mathbf{E}_1$, $\mathbf{E}_2$ and $\mathbf{E}_3$, while $\Theta \in [0, \pi]$ and $\Phi \in [0, 2\pi]$ are spherical polar angles.

where ρ, which now depends only on Θ, is the fiber orientation density, rotationally symmetric about the mean fiber direction **M** from which the angle Θ is measured; see Fig. 1, in which $\mathbf{E}_1$, $\mathbf{E}_2$ and $\mathbf{E}_3 = \mathbf{M}$ are rectangular Cartesian coordinates and $\Theta \in [0, \pi]$ and $\Phi \in [0, 2\pi]$ are spherical polar angles. A general unit vector **N** is defined in terms of Θ and Φ by

$$\mathbf{N} = \sin\Theta\cos\Phi\,\mathbf{E}_1 + \sin\Theta\sin\Phi\,\mathbf{E}_2 + \cos\Theta\,\mathbf{E}_3. \tag{13}$$

Note that κ is normally restricted to the interval $[0, 1/3]$, with $\kappa = 0$ corresponding to the case with no dispersion (in which limit ρ is a delta function) and $\kappa = 1/3$ to an isotropic dispersion in 3D with fibers equally distributed in all directions (and $\rho \equiv 1$), as detailed in, for example, [10]. It is in principle possible for κ to lie in the interval $[1/3, 1/2]$, with $\kappa = 1/2$ associated with a 2D isotropic dispersion, but in 3D this interval can sometimes yield unphysical results, as shown in [27].

The normalization condition (2) reduces to

$$\frac{1}{2}\int_0^\pi \rho(\Theta)\sin\Theta \mathrm{d}\Theta = 1 \tag{14}$$

with $\rho(\Theta)$ having the symmetry properties

$$\rho(\pi + \Theta) = \rho(\pi - \Theta) = \rho(\Theta). \tag{15}$$

With the generalized structure tensor (11), and the definitions in (7), the generalized invariants $I_4^\star$ and $I_5^\star$ become

$$I_4^\star = \kappa I_1 + (1 - 3\kappa)I_4(\mathbf{M}), \qquad I_5^\star = \kappa(I_1^2 - 2I_2) + (1 - 3\kappa)I_5(\mathbf{M}), \tag{16}$$

where I_1 and I_2 are defined in (5), and $I_4(\mathbf{M})$ and $I_5(\mathbf{M})$ in (6) with $\mathbf{N}$ replaced by $\mathbf{M}$.

As an example, we now consider the energy function

$$\Psi_{\mathrm{GST}} = \Psi_{\mathrm{f}}(I_4^\star) + \Psi_{\mathrm{iso}}(I_1), \tag{17}$$

from which the Cauchy stress tensor (10) is given by

$$\boldsymbol{\sigma}_{\mathrm{GST}} = 2\Psi_{\mathrm{f}}'(I_4^\star)\mathbf{h} + 2\psi_{\mathrm{iso}\,1}\mathbf{B} - p\mathbf{I}, \tag{18}$$

where a prime here denotes the derivative with respect to the argument of the considered function, and

$$\mathbf{h} = \mathbf{F}\mathbf{H}\mathbf{F}^{\mathrm{T}} = \kappa\mathbf{B} + (1-3\kappa)\mathbf{m}\otimes\mathbf{m} \tag{19}$$

is the spatial version of the structure tensor $\mathbf{H}$ introduced in (11), and it is worth noting that $I_4^\star = \mathrm{tr}\mathbf{h}$. There is no corresponding simple expression for $\boldsymbol{\sigma}_{\mathrm{AI}}$ since the integrand in eq. (9) depends on Θ and Φ through λ, $\mathbf{N}$ and $\mathbf{n}$ in general.

A particular example of (17), which we use later, is the simple model for one family of fibers for which

$$\Psi_{\mathrm{iso}}(I_1) = \frac{\mu}{2}(I_1-3), \quad \Psi_{\mathrm{f}}(I_4^\star) = \frac{k_1}{2k_2}\left\{\exp\left[k_2(I_4^\star-1)^2\right]-1\right\}, \tag{20}$$

where μ, k_1 and k_2 are positive material parameters. It is composed of the neo-Hookean model Ψ_{iso} and an exponential model Ψ_{f}. From (18), the Cauchy stress tensor then becomes

$$\boldsymbol{\sigma}_{\mathrm{GST}} = 2k_1(I_4^\star-1)\exp[k_2(I_4^\star-1)^2]\mathbf{h} + \mu\mathbf{B} - p\mathbf{I}. \tag{21}$$

If there are two fiber families with the second family having a mean direction $\mathbf{M}'$, with generalized structure tensors $\mathbf{H}' = \kappa'\mathbf{I} + (1-3\kappa')\mathbf{M}'\otimes\mathbf{M}'$ and $\mathbf{h}' = \mathbf{F}\mathbf{H}'\mathbf{F}^{\mathrm{T}}$, $\mathbf{m}' = \mathbf{F}\mathbf{M}'$, $I_6 = \mathbf{m}'\cdot\mathbf{m}'$, then the Cauchy stress tensor (21) extends to

$$\boldsymbol{\sigma}_{\mathrm{GST}} = 2k_1(I_4^\star-1)\exp[k_2(I_4^\star-1)^2]\mathbf{h} + 2k_1'(I_6^\star-1)\exp[k_2'(I_6^\star-1)^2]\mathbf{h}' + \mu\mathbf{B} - p\mathbf{I}, \tag{22}$$

where κ' is the dispersion parameter associated with the second fiber family, and k_1' and k_2' are the counterparts of k_1 and k_2 for the second family. Likewise, this could be extended to multiple fiber families and non-symmetric dispersion.

Correspondingly, for comparison, suppose that $w(\lambda)$ has the exponential form

$$w(\lambda) = \frac{c_1}{2c_2}\{\exp[c_2(\lambda^2-1)^2]-1\}, \tag{23}$$

where c_1 and c_2 are constants. Then with $(20)_1$, the formula (9) specializes to

$$\boldsymbol{\sigma}_{\mathrm{AI}} = 2nc_1\int_\Omega \rho(\mathbf{N})(\lambda^2-1)\exp[c_2(\lambda^2-1)^2]\mathbf{n}\otimes\mathbf{n}\mathrm{d}\Omega + \mu\mathbf{B} - p\mathbf{I}, \tag{24}$$

where $\mathrm{d}\Omega = \sin\Theta\mathrm{d}\Theta\mathrm{d}\Phi$. If, in particular, $\rho(\mathbf{N})$ is symmetric about a mean direction $\mathbf{M}$ then ρ depends on $\mathbf{N}$ through $\mathbf{N}\cdot\mathbf{M}$. Note that without loss of generality n can be absorbed into c_1.

4 Representative examples

4.1 Simple tension

We start by considering a uniaxial stretch $\lambda_3 \geq 1$ in the direction $\mathbf{M}\,(=\mathbf{E}_3)$ with a rotationally symmetric dispersion about $\mathbf{M}$, and for the GST model a single family of fibers. By symmetry, the lateral stretches $\lambda_1 = \lambda_2$ are $\lambda_3^{-1/2}$ so that the matrix of the components of $\mathbf{F}$ is $\mathrm{diag}[\lambda_3^{-1/2}, \lambda_3^{-1/2}, \lambda_3]$. For a general direction $\mathbf{N}$, given by (13), we obtain the stretch $\lambda = \sqrt{\mathbf{N}\cdot\mathbf{C}\mathbf{N}}$ as

$$\lambda = \sqrt{\lambda_3^2\cos^2\Theta + \lambda_3^{-1}\sin^2\Theta}, \tag{25}$$

which is independent of Φ. Hence, from (9) we obtain, on performing the integration with respect to Φ and using the connection $\mathbf{E}_1\otimes\mathbf{E}_1 + \mathbf{E}_2\otimes\mathbf{E}_2 + \mathbf{E}_3\otimes\mathbf{E}_3 = \mathbf{I}$,

$$\boldsymbol{\sigma}_{\mathrm{AI}} = \pi n\int_0^\pi \rho(\Theta)\lambda^{-1}w'(\lambda)(2\lambda_3^2\cos^2\Theta - \lambda_3^{-1}\sin^2\Theta)\sin\Theta\mathrm{d}\Theta\,\mathbf{E}_3\otimes\mathbf{E}_3 + \mu\mathbf{B} - \bar{p}\mathbf{I}, \tag{26}$$

where the form of Ψ_{iso} given in eq. $(20)_1$ has been used together with the expression (13) for $\mathbf{N}$, and $\mathbf{n} = \mathbf{F}\mathbf{N}$. In (26) the notation

$$\bar{p} = p - \pi n\lambda_3^{-1}\int_0^\pi \rho(\Theta)\lambda^{-1}w'(\lambda)\sin^3\Theta\mathrm{d}\Theta \tag{27}$$

has been introduced. For simple tension with $\sigma_{\mathrm{AI}\,11} = \sigma_{\mathrm{AI}\,22} = 0$ we then obtain

$$\sigma_{\mathrm{AI}\,33} = \pi n\int_0^\pi \rho(\Theta)\lambda^{-1}w'(\lambda)(2\lambda_3^2\cos^2\Theta - \lambda_3^{-1}\sin^2\Theta)\sin\Theta\mathrm{d}\Theta + \mu(\lambda_3^2 - \lambda_3^{-1}), \tag{28}$$

and there are no shear stress components.

We now consider the specific kinematics in order to find the Cauchy stress $\sigma_{\mathrm{GST}\,33}$ for the GST model. First we need to compute $\mathbf{h}$ and $I_4^\star$ from (19) and $(16)_1$, respectively, which give

$$\mathbf{h} = \kappa\lambda_3^{-1}\mathbf{I} + [\lambda_3^2(1-2\kappa) - \kappa\lambda_3^{-1}]\mathbf{E}_3\otimes\mathbf{E}_3, \quad I_4^\star = \lambda_3^2 - 2\kappa(\lambda_3^2 - \lambda_3^{-1}). \tag{29}$$

The non-zero components of $\mathbf{h}$ are $h_{11} = h_{22} = \kappa\lambda_3^{-1}$ and $h_{33} = \lambda_3^2(1-2\kappa)$. Then, from (21), we reduce the stress in the direction of the applied stretch λ_3 to

$$\begin{aligned}\sigma_{\mathrm{GST}\,33} = {}& 2k_1[\lambda_3^2 - 1 - 2\kappa(\lambda_3^2 - \lambda_3^{-1})](\lambda_3^2 - 2\kappa\lambda_3^2 - \kappa\lambda_3^{-1})\\ & \times\exp\left\{k_2[\lambda_3^2 - 1 - 2\kappa(\lambda_3^2 - \lambda_3^{-1})]^2\right\} + \mu(\lambda_3^2 - \lambda_3^{-1}),\end{aligned} \tag{30}$$

where the Lagrange multiplier p has been eliminated by use of $\sigma_{\mathrm{GST}\,11} = \sigma_{\mathrm{GST}\,22} = 0$.

A possible way to describe the fiber dispersion is by the use of the von Mises distribution of the form [28]

$$\rho(\Theta) = 4\sqrt{\frac{b}{2\pi}}\frac{\exp(2b\cos^2\Theta)}{\mathrm{erfi}(\sqrt{2b})}, \tag{31}$$

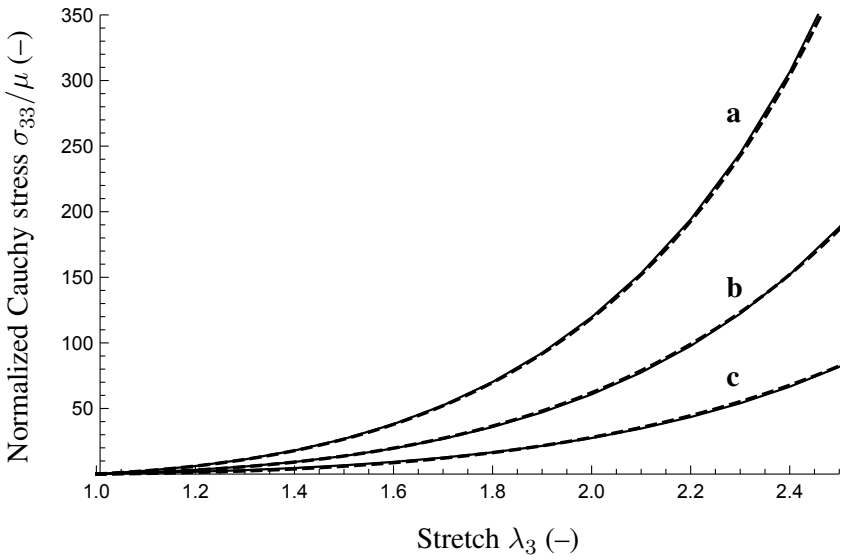

Figure 2: Comparison of the GST (dashed curves) and AI (solid curves) predictions for simple tension for the normalized uniaxial stress σ_{33}/μ against the stretch λ_3 for three different dispersions. The plots are based on the eqs. (30) and (28), respectively. The parameters for the three pairs of curves are provided in the text.

where erfi is the imaginary error function and b is the concentration parameter. By substituting (31) in the definition (12) and using MATHEMATICA [29] we obtain a specific expression for the dispersion parameter κ, i.e.

$$\kappa = \frac{1}{2} + \frac{1}{8b} - \frac{1}{4}\sqrt{\frac{2}{\pi b}}\frac{\exp(2b)}{\mathrm{erfi}(\sqrt{2b})}. \tag{32}$$

Plots of the AI model prediction of the normalized Cauchy stress σ_{33}/μ versus the stretch λ_3 for simple tension, which are based on eq. (28) with (23), are shown as solid curves in Fig. 2 for parameter values $nc_1 = 5$ and $c_2 = 0.01$ in each case. For the three curves the concentration parameter b is taken to be 10 for curve **a**, 1.5 for curve **b**, and 0.1 for curve **c**. For comparison the dashed curves are calculated for the GST model based on eq. (30), with $k_2 = 0.01$ in each case, while for curve **a** $k_1 = 5$, $\kappa = 0.026$, for curve **b** $k_1 = 5.3$, $\kappa = 0.15$, and for curve **c** $k_1 = 5.7$, $\kappa = 0.26$. In order to compute the integrals in (28) for the plotting, MATHEMATICA [29] was used.

As can be seen from Fig. 2 both models are able to provide the same uniaxial stress versus stretch curves. This is in complete contrast to the flawed comparative study in [21].

4.2 Fitting to tissue data

We now consider the two models in relation to uniaxial data from two orthogonal directions obtained from the adventitia of a human non-atherosclerotic abdominal aorta [11]. It is assumed that the tests take place in the $(1,2)$ plane with corresponding principal stretches λ_1 and λ_2. For the GST model we consider two families of fibers with equal properties ($\kappa' = \kappa$, $k_1' = k_1$, $k_2' = k_2$) and with mean fiber directions in the $(1,2)$ plane, symmetrically disposed with respect to the $(1,2)$ axes. We therefore take

$$\mathbf{M} = \cos\alpha\mathbf{E}_1 + \sin\alpha\mathbf{E}_2, \quad \mathbf{M}' = \cos\alpha\mathbf{E}_1 - \sin\alpha\mathbf{E}_2, \tag{33}$$

where the angle α defines the orientation of the mean fiber directions relative to the $\mathbf{E}_1$ direction. Then,

$$\mathbf{m} = \lambda_1\cos\alpha\mathbf{E}_1 + \lambda_2\sin\alpha\mathbf{E}_2, \quad \mathbf{m}' = \lambda_1\cos\alpha\mathbf{E}_1 - \lambda_2\sin\alpha\mathbf{E}_2, \tag{34}$$

and it follows that $I_1 = \lambda_1^2 + \lambda_2^2 + \lambda_1^{-2}\lambda_2^{-2}$ and $I_4 = I_6 = \lambda_1^2\cos^2\alpha + \lambda_2^2\sin^2\alpha$, and, according to $(16)_1$,

$$I_4^\star = I_6^\star = \kappa(\lambda_1^2 + \lambda_2^2 + \lambda_1^{-2}\lambda_2^{-2}) + (1-3\kappa)(\lambda_1^2\cos^2\alpha + \lambda_2^2\sin^2\alpha). \tag{35}$$

Hence, from $(29)_1$, $h_{11}' = h_{11}$, $h_{22}' = h_{22}$, $h_{12}' = -h_{12}$, and by specializing (22) and eliminating p using $\sigma_{\mathrm{GST}\,33} = 0$, the in-plane normal stresses become

$$\sigma_{\mathrm{GST}\,11} = (\xi\kappa + \mu)(\lambda_1^2 - \lambda_3^2) + \xi(1-3\kappa)\lambda_1^2\cos^2\alpha, \tag{36}$$

$$\sigma_{\mathrm{GST}\,22} = (\xi\kappa + \mu)(\lambda_2^2 - \lambda_3^2) + \xi(1-3\kappa)\lambda_2^2\sin^2\alpha, \tag{37}$$

where the notation $\xi = 4k_1(I_4^\star - 1)\exp[k_2(I_4^\star - 1)^2]$ has been introduced, and by symmetry there is no shear stress ($\sigma_{\mathrm{GST}\,12} = 0$).

Next, we derive the corresponding equations for the AI model. The deformation gradient $\mathbf{F}$ is diagonal with respect to the Cartesian axes according to $\mathbf{F} = \mathrm{diag}[\lambda_1, \lambda_2, \lambda_3]$. For $\mathbf{n} = \mathbf{F}\mathbf{N}$, using (13), we obtain

$$\mathbf{n} = \lambda_1\sin\Theta\cos\Phi\mathbf{E}_1 + \lambda_2\sin\Theta\sin\Phi\mathbf{E}_2 + \lambda_3\cos\Theta\mathbf{E}_3, \tag{38}$$

and, consequently, $\lambda^2 = \mathbf{n}\cdot\mathbf{n}$ is

$$\lambda^2 = \sin^2\Theta(\lambda_1^2\cos^2\Phi + \lambda_2^2\sin^2\Phi) + \lambda_3^2\cos^2\Theta. \tag{39}$$

Next the form of the distribution $\rho(\mathbf{N})$ needs to be considered. In general, for a mean fiber direction $\mathbf{M}$, as given above, the von Mises distribution (31) is adjusted to

$$\rho(\mathbf{N}) = 4\sqrt{\frac{b}{2\pi}}\frac{\exp[2b(\mathbf{N}\cdot\mathbf{M})^2]}{\mathrm{erfi}(\sqrt{2b})}, \tag{40}$$

where

$$\mathbf{N}\cdot\mathbf{M}=\sin\Theta\cos(\Phi-\alpha), \tag{41}$$

for which the expressions (13) and (33) have been used. However, to avoid shear stresses and to capture the general biaxial deformation with just the two in-plane normal stresses, ρ should be symmetric about both $\mathbf{E}_1$ and $\mathbf{E}_2$, so that, when considering ρ as a function of Θ and Φ we must have

$$\rho(\Theta,2\pi-\Phi)=\rho(\Theta,\pi-\Phi)=\rho(\Theta,\Phi). \tag{42}$$

This can be met by taking either $\alpha=0$ or $\alpha=\pi/2$. For definiteness, we take $\alpha=0$. Then all the shear components in (24) vanish, and the normal components are given by

$$\sigma_{\mathrm{AI}\,11}=2\lambda_1^2nc_1\int_\Omega\beta\cos^2\Phi\sin^3\Theta\mathrm{d}\Theta\mathrm{d}\Phi+\mu\lambda_1^2-p, \tag{43}$$

$$\sigma_{\mathrm{AI}\,22}=2\lambda_2^2nc_1\int_\Omega\beta\sin^2\Phi\sin^3\Theta\mathrm{d}\Theta\mathrm{d}\Phi+\mu\lambda_2^2-p, \tag{44}$$

$$\sigma_{\mathrm{AI}\,33}=2\lambda_3^2nc_1\int_\Omega\beta\cos^2\Theta\sin\Theta\mathrm{d}\Theta\mathrm{d}\Phi+\mu\lambda_3^2-p, \tag{45}$$

where the notation

$$\beta=\rho(\mathbf{N})(\lambda^2-1)\exp[c_2(\lambda^2-1)^2] \tag{46}$$

has been introduced, and λ^2 is given by (39).

By eliminating the hydrostatic pressure p from (43) and (44) by using the condition $\sigma_{\mathrm{AI}\,33}=0$, we get

$$\sigma_{\mathrm{AI}\,11}=2nc_1\int_\Omega\beta(\lambda_1^2\cos^2\Phi\sin^2\Theta-\lambda_3^2\cos^2\Theta)\sin\Theta\mathrm{d}\Theta\mathrm{d}\Phi+\mu(\lambda_1^2-\lambda_3^2), \tag{47}$$

$$\sigma_{\mathrm{AI}\,22}=2nc_1\int_\Omega\beta(\lambda_2^2\sin^2\Phi\sin^2\Theta-\lambda_3^2\cos^2\Theta)\sin\Theta\mathrm{d}\Theta\mathrm{d}\Phi+\mu(\lambda_2^2-\lambda_3^2), \tag{48}$$

which are the analogues of $\sigma_{\mathrm{GST}\,11}$ and $\sigma_{\mathrm{GST}\,22}$ listed in (36) and (37), respectively.

Equations (36), (37), (47) and (48) are appropriate for general biaxial deformations. However, it suffices to fit the two models to representative experimental data from uniaxial extension tests presented in [11], rather than biaxial tests. Equations (36) and (37) are used respectively for the axial and circumferential directions, with measured values of the appropriate lateral stretches. Likewise, for eqs. (47) and (48).

We now fit the two models to representative experimental data from uniaxial tension tests on the adventitia of a human non-atherosclerotic abdominal aorta [11]. The tests were performed on orthogonal strips of the tissue taken from nearby positions. The experimental data are presented as solid dots in Fig. 3. The response of the strip aligned in the axial direction is

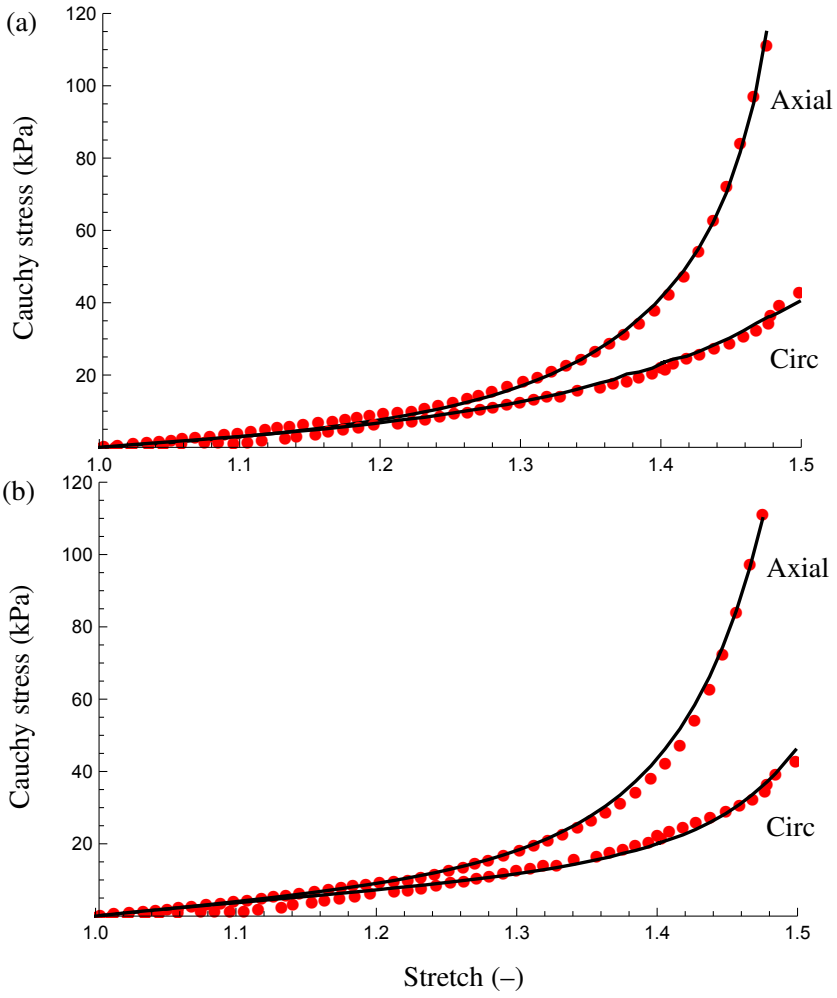

Figure 3: Comparison of experimental data (solid dots) obtained from the adventitia of a human non-atherosclerotic abdominal aorta [11] with model predictions (solid curves): (a) GST model; (b) AI model. The individual parameters for the two constitutive models are provided in the text.

stiffer than that aligned with the circumferential direction. The two sets of data are fitted by the GST model with the same set of parameters, which are given by $\kappa = 0.3$, $c = 7.267\,\text{kPa}$, $k_1 = 54.11\,\text{kPa}$, $k_2 = 20.41$ and $\alpha = \pi/8$, while the AI model yields the parameters $b = 0.95$, $\mu = 8.5\,\text{kPa}$, $c_1 = 0.59\,\text{kPa}$, $c_2 = 2.15$ and $\alpha = 0$. MATHEMATICA [29] was used for the fitting. For the GST model the correlation coefficients for the axial and circumferential data were obtained as 0.999 and 0.998, while for the AI model they were 0.999 and 0.994, respectively. The fits of the two models in Fig. 3 illustrate the Cauchy stress (in kPa) versus stretch by the solid curves, for the GST model in (a) and for the AI model in (b). In each case σ_{11} is plotted against λ_1 for the axial strip, while σ_{22} versus λ_2 is shown for the circumferential strip. As can be seen,

the agreement of both models with the experimental data is very satisfactory.

4.3 Simple shear in the $(1,2)$ plane

In the next example we consider simple shear in the $(\mathbf{E}_1, \mathbf{E}_2)$ plane in the $\mathbf{E}_1$ direction, with a dispersion for which the fibers are all located in this plane, with an arbitrary fiber direction $\mathbf{N}$ having the form

$$\mathbf{N} = \cos\Theta\mathbf{E}_1 + \sin\Theta\mathbf{E}_2, \tag{49}$$

where the polar angle Θ is different from the Θ used in Fig. 1, and it satisfies $-\pi/2 \leq \Theta \leq \pi/2$. Let the mean fiber direction be denoted by $\mathbf{M}$ in the considered plane according to the relation $(33)_1$, with a single family of fibers for the GST model. The components of the deformation gradient $\mathbf{F}$ are, in matrix notation,

$$[\mathbf{F}] = \begin{bmatrix} 1 & \gamma & 0 \\ 0 & 1 & 0 \\ 0 & 0 & 1 \end{bmatrix}, \tag{50}$$

where $\gamma \geq 0$ denotes the amount of shear. The stretch λ in the direction $\mathbf{N}$ is then given by

$$\lambda^2 = \mathbf{n}\cdot\mathbf{n} = 1 + \gamma\sin\Theta(\gamma\sin\Theta + 2\cos\Theta), \tag{51}$$

where $\mathbf{n} = \mathbf{F}\mathbf{N} = \mathbf{N} + \gamma(\mathbf{N}\cdot\mathbf{E}_2)\mathbf{E}_1$, and we assume that $\Psi_{\rm iso}$ is again the neo-Hookean model $(20)_1$. Since attention is now being confined to the $(1,2)$ plane we introduce a superposed hat to indicate this, so that, e.g., $\hat{\mathbf{F}}$ is the restriction of $\mathbf{F}$ to the $(1,2)$ plane. From (9) specialized to two dimensions we obtain

$$\hat{\boldsymbol{\sigma}}_{\rm AI} = \hat{n}\int_{-\pi/2}^{\pi/2}\rho(\Theta)\lambda^{-1}w'(\lambda)\mathbf{n}\otimes\mathbf{n}\mathrm{d}\Theta + \mu\hat{\mathbf{B}} - p\hat{\mathbf{I}}, \tag{52}$$

where $\hat{n}$ is here the number of fibers per unit reference area, $\hat{\mathbf{B}} = \hat{\mathbf{F}}\hat{\mathbf{F}}^{\rm T}$, and $\hat{\mathbf{I}}$ is the two-dimensional identity. Note that the hat is not needed on $\mathbf{N}$ or $\mathbf{n}$ because they are two-dimensional (2D) anyway.

In particular, the in-plane shear stress is given by

$$\hat{\sigma}_{\rm AI\,12} = \hat{n}\int_{-\pi/2}^{\pi/2}\rho(\Theta)\lambda^{-1}w'(\lambda)(\cos\Theta + \gamma\sin\Theta)\sin\Theta\mathrm{d}\Theta + \mu\gamma. \tag{53}$$

We now use the GST model and continue by assuming the symmetry $\rho(\Theta+\pi) = \rho(\Theta)$ for the 2D dispersion with $\rho(\Theta)$ satisfying the normalization condition

$$\frac{1}{\pi}\int_{-\pi/2}^{\pi/2}\rho(\Theta)\mathrm{d}\Theta = 1. \tag{54}$$

The 2D generalized structure tensor has the form [27]

$$\hat{\mathbf{H}} = \kappa\hat{\mathbf{I}} + (1-2\kappa)\mathbf{M}\otimes\mathbf{M}, \tag{55}$$

where κ is the associated dispersion parameter defined by

$$\kappa = \frac{1}{\pi}\int_{-\pi/2}^{\pi/2}\rho(\Theta)\sin^2\Theta\mathrm{d}\Theta, \tag{56}$$

which is analogous to (12), but we have not included a superposed hat in this case. The value of κ defined in (56) is independent of $\mathbf{M}$ for a dispersion which is symmetric about $\mathbf{M}$. For the 2D version of the von Mises distribution, $\rho(\Theta)$ has the form

$$\rho(\Theta) = \frac{\exp(b\cos 2\Theta)}{I_0(b)}, \tag{57}$$

where I_0 is the modified Bessel function of the first kind of order 0. Then, by substituting (57) into (56) and using MATHEMATICA [29] the associated dispersion parameter κ is given by [11]

$$\kappa = \frac{1}{2}\left(1-\frac{I_1(b)}{I_0(b)}\right), \tag{58}$$

where $I_1(b)$ is the modified Bessel function of the first kind of order 1. Note that in 2D κ lies in the interval $[0, 1/2]$.

Consider the model Ψ_{GST}, given by (17), specialized to the plane strain case. The 2D Cauchy stress is obtained by specializing (18) to give

$$\hat{\boldsymbol{\sigma}}_{\mathrm{GST}} = 2\Psi_{\mathrm{f}}'(I_4^\star)\hat{\mathbf{h}} + 2\psi_{\mathrm{iso}\,1}\hat{\mathbf{B}} - p\hat{\mathbf{I}}, \tag{59}$$

with $\hat{\mathbf{h}} = \kappa\hat{\mathbf{B}}+(1-2\kappa)\mathbf{m}\otimes\mathbf{m}$. With (50) and $[\mathbf{M}] = [M_1,\, M_2,\, 0]^{\mathrm{T}}$ the components of $\mathbf{m} = \mathbf{FM}$ are $m_1 = M_1 + \gamma M_2$, $m_2 = M_2$, $m_3 = M_3 = 0$, where $M_1 = \cos\alpha$ and $M_2 = \sin\alpha$. The associated in-plane invariants are

$$\hat{I}_1 = \mathrm{tr}\hat{\mathbf{B}} = 2+\gamma^2, \qquad \hat{I}_4^\star = \mathrm{tr}\hat{\mathbf{h}} = \kappa(2+\gamma^2) + (1-2\kappa)(1+2\gamma M_1M_2+\gamma^2M_2^2), \tag{60}$$

where $M_1^2 + M_2^2 = 1$ has been used. The strain-energy function (17), with Ψ_{f} and Ψ_{iso} given by (20), has the same form with I_1 and $I_4^\star$ replaced by $\hat{I}_1 + 1$ and $\hat{I}_4^\star$, respectively. Hence, from (59), the Cauchy shear stress component is given by

$$\hat{\sigma}_{\mathrm{GST}\,12} = \mu\gamma + 2\Psi_{\mathrm{f}}'(I_4^\star)[\kappa\gamma + (1-2\kappa)(M_1+\gamma M_2)M_2]. \tag{61}$$

Plots of the normalized shear stress $\hat{\sigma}_{12}/\mu$ against the amount of shear γ for the AI model prediction for simple shear in the $(1,2)$ plane, which are based on (53), are shown as solid

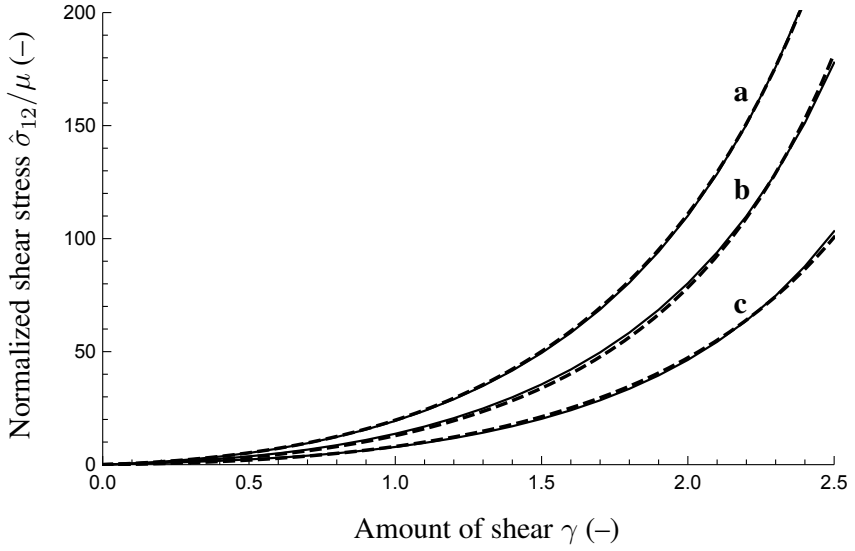

Figure 4: Comparison of GST (dashed curves) and AI (solid curves) predictions for simple shear for the normalized shear stress $\hat{\sigma}_{12}/\mu$ against the amount of shear γ for three different dispersions. The plots are based on the eqs. (53) and (61). The parameters for the three pairs of curves are provided in the text.

curves in Fig. 4 for parameter values $\hat{n}c_1 = 5$, $c_2 = 0.01$ in each case. For the three curves the concentration parameter $b = 10$ for the curve **a**, 1.5 for the curve **b**, and 0.1 for the curve **c**. For comparison the dashed curves are calculated for the GST model based on (61). For the curve **a** $\kappa = 0.026$, $k_1 = 5.1$, $k_2 = 0.01$, for the curve **b** $\kappa = 0.15$, $k_1 = 4.6$, $k_2 = 0.0163$ and for the curve **c** $\kappa = 0.26$, $k_1 = 4.05$ and $k_2 = 0.014$. The angle α was taken to be $\pi/3$.

Similarly to the case of simple tension both models are able to provide the same shear stress versus amount of shear curves.

5 Linearized model comparison

So far we have considered the nonlinear case and have shown that the two different models are able to recover the same mechanical response, even though theoretically they are not the same. Indeed, even in the linear theory they do not coincide, and we now emphasize this by restricting attention to the linear theory. We start by referring to the strain-energy function (1) but with the Ψ_{iso} term omitted. Since $w(1) = 0$ the Taylor expansion of $w = w(\lambda)$ gives

$$w(\lambda) = (\lambda - 1)w'(1) + \frac{1}{2}(\lambda - 1)^2 w''(1) + \dots, \tag{62}$$

where $w'(1) = 0$ if there is no residual stress. In addition, we have $I_4 - 1 = \mathbf{N} \cdot (\mathbf{CN}) - 1 = 2\mathbf{N} \cdot (\mathbf{EN})$, where $\mathbf{E} = (\mathbf{C} - \mathbf{I})/2$ denotes the Green–Lagrange strain tensor, and hence

$$\lambda = 1 + \mathbf{N} \cdot (\mathbf{EN}) - \frac{1}{2}[\mathbf{N} \cdot (\mathbf{EN})]^2 + \dots \tag{63}$$

to the second order in $\mathbf{E}$. By substituting (62) and (63) into (1) we obtain

$$\Psi_{\mathrm{AI}} = 4\pi n w'(1)\mathbf{H} : \mathbf{E} + 2\pi n[w''(1) - w'(1)]\mathbf{E} : \boldsymbol{\mathcal{H}} : \mathbf{E} + \dots, \tag{64}$$

where $\mathbf{H}$ is defined in (3) and the fourth-order structure tensor $\boldsymbol{\mathcal{H}}$ is given by

$$\boldsymbol{\mathcal{H}} = \frac{1}{4\pi} \int_\Omega \rho(\mathbf{N}) \mathbf{N} \otimes \mathbf{N} \otimes \mathbf{N} \otimes \mathbf{N} \mathrm{d}\Omega. \tag{65}$$

The related index notation reads

$$H_{ij} = \frac{1}{4\pi} \int_\Omega \rho N_i N_j \mathrm{d}\Omega, \qquad \mathcal{H}_{ijkl} = \frac{1}{4\pi} \int_\Omega \rho N_i N_j N_k N_l \mathrm{d}\Omega. \tag{66}$$

Note that $\mathcal{H}_{ijkl}$ has complete i, j, k, l symmetry and satisfies (in the summation convention)

$$\mathcal{H}_{iijj} = 1, \qquad \mathcal{H}_{11jj} = \mathcal{H}_{22jj} = \kappa, \qquad \mathcal{H}_{33jj} = 1 - 2\kappa, \tag{67}$$

where $(67)_1$ was obtained by using the normalization condition (2), and $(67)_2$ and $(67)_3$ by using (11) with $\mathbf{M} = \mathbf{E}_3$. The only non-zero components of $\mathcal{H}_{ijkl}$ are

$$\mathcal{H}_{1111} = \mathcal{H}_{2222} = 3\mathcal{H}_{1122} = \frac{3}{4}\kappa_1, \quad \mathcal{H}_{1133} = \mathcal{H}_{2233} = \kappa - \kappa_1, \quad \mathcal{H}_{3333} = 1 - 4\kappa + 2\kappa_1, \tag{68}$$

where the additional dispersion parameter

$$\kappa_1 = \frac{1}{4} \int_0^\pi \rho(\Theta) \sin^5 \Theta \mathrm{d}\Theta \tag{69}$$

has been introduced. The relations (68) are obtained by using the components of $\mathbf{N}$ given in (13), carrying out the integration over Φ, and using (12) and (14).

For the GST approach we use (4), again without Ψ_{iso}, so that the Taylor series expansion of Ψ_{GST}, with $\Psi_{\mathrm{f}}(\mathbf{I}, \mathbf{H}) = 0$, gives

$$\Psi_{\mathrm{GST}} = \frac{\partial \Psi_{\mathrm{f}}(\mathbf{I}, \mathbf{H})}{\partial \mathbf{C}} : (\mathbf{C} - \mathbf{I}) + \frac{1}{2} \left[\frac{\partial^2 \Psi_{\mathrm{f}}(\mathbf{I}, \mathbf{H})}{\partial \mathbf{C}^2} (\mathbf{C} - \mathbf{I}) \right] : (\mathbf{C} - \mathbf{I}) + \dots \tag{70}$$

By assuming the simple energy function $\Psi_{\mathrm{f}} = \Psi_{\mathrm{f}}(I_4^\star)$, with $I_4^\star = \kappa I_1 + (1 - 3\kappa) I_4$ and the Green–Lagrange strain tensor $\mathbf{E}$ we obtain

$$\Psi_{\mathrm{GST}} = 2\Psi_{\mathrm{f}}'(1)\mathbf{H} : \mathbf{E} + 2\Psi_{\mathrm{f}}''(1)(\mathbf{H} : \mathbf{E})^2 + \dots, \tag{71}$$

where $\mathbf{H}$ is defined in (11) for fibers distributed with rotational symmetry about the mean direction $\mathbf{M}$, and $\Psi_{\rm f}'(1) = 0$ if there is no residual stress.

It is now straightforward to calculate the second Piola–Kirchhoff stress tensor $\mathbf{S}_{\rm AI}$ for the AI model and $\mathbf{S}_{\rm GST}$ for the GST model. By recalling (64) and (71) we obtain

$$\mathbf{S}_{\rm AI} = \frac{\partial \Psi_{\rm AI}}{\partial \mathbf{E}} = 4\pi n w'(1)\mathbf{H} + 4\pi n[w''(1) - w'(1)]\boldsymbol{\mathcal{H}} : \mathbf{E} + \ldots, \tag{72}$$

$$\mathbf{S}_{\rm GST} = \frac{\partial \Psi_{\rm GST}}{\partial \mathbf{E}} = 2\Psi_{\rm f}'(1)\mathbf{H} + 4\Psi_{\rm f}''(1)(\mathbf{H} : \mathbf{E})\mathbf{H} + \ldots. \tag{73}$$

From these two equations it can be seen immediately that even when linearized the two models are not in general the same. In particular, the $\boldsymbol{\mathcal{H}}$ tensor involves κ_1 and κ, whereas $\mathbf{H}$ involves only κ.

6 Discussion

In this paper we have compared the predictions of the two main modeling approaches that are used for the description of the elastic properties of fiber-reinforced materials with dispersed fibers, in particular of soft biological tissues such as arterial walls and cartilages. For each of the models the fibers are considered to be embedded within an isotropic matrix, for which the elastic properties are modeled as a neo-Hookean material. For the GST model the properties of the dispersed collagen fibers are captured by an exponential strain-energy function based on generalized structure tensors, with the dispersion symmetrically arranged around the mean fiber direction for each fiber family [10]. For the AI model, on the other hand, following Lanir [15], the elastic properties of the individual fibers, modeled with an exponential function and weighted by an orientation density, are aggregated into an overall fiber-energy function by integrating over a unit sphere.

An important aim of this paper has been to show that the predictive powers of the GST and AI models are essentially equivalent. In particular, we have shown that for both simple tension and simple shear the predictions of the two dispersion models are virtually identical for a significant range of large deformations, which is in sharp contrast with flawed comparisons in the literature (see, in particular, [20, 21]). In a third example, we have fitted each dispersion model to experimental data obtained from uniaxial extension tests on human tissue samples taken from along the circumferential and axial directions of an artery [11]. Excellent fits have been obtained with both models. However, while the GST model has been used to fit data from a wide range of tissues, corresponding fits to real data for the AI model are still rare. This is partly due to the integrations involved in the AI model, which require more computational effort

compared with the fit of the GST model to real data. To the authors' knowledge fitting of the AI model to real data has been limited to the fitting of uniaxial and biaxial data of native bovine pericardium using a simple constitutive law for the fibers and a planar orientation distribution [30]. However, this particular constitutive model has not been used within a finite element environment. The problem with the AI approach is compounded in respect of finite element computations of realistic boundary-value problems, as is well known. Indeed, because of this issue, the AI model has not yet been implemented in commercial finite element software. One important consideration for a model of soft biological tissues is its ability to exclude fibers that are under compression. As we have shown in the study [18], the numerical integration (over a subset of the unit sphere) becomes very costly if the AI approach is implemented with compressed fibers excluded.

The dispersion parameter for a single family of fibers has a clear physical interpretation and can be determined from measurements of the fiber orientation density. This physical interpretation is carried by the specific form of the GST model used in this study which involves just a single dispersion parameter. Once the mean fiber direction and the orientation density are known, the generalized structure tensor is then determined once and for all, and no further integration is then needed. The GST approach is very flexible and can be extended to accommodate multiple families of fibers with different mean directions and dispersions. In addition, coupling between fibers in different families can be included in the model by means of a coupling invariant $(\mathbf{M} \cdot \mathbf{CM}')^2$. The AI model, which provides an attractive theoretical framework, integrates the energy stored in an individual fiber weighted by an orientation density function, and can accommodate different fiber properties by using different energy functions. Such integrations, however, need to be performed at every Gauss point within a finite element realization, and are expensive in CPU time. The present study illustrates that theoretically either model can be used to represent the response of fibrous materials, but adoption of the AI model remains problematic from the computational efficiency point of view.

To summarize, the AI approach is certainly an attractive formulation, but it does not appear to offer any advantages over the GST approach. Advantages of the GST approach include (1) it is an algebraic formulation and is therefore easier to implement than the AI formulation, (2) it admits explicit analytical results for a range of different deformations, which is not the case for the AI approach, (3) the numerical analysis is less costly, in particular if compressed fibers are excluded, and (4) it is more accurate since the numerical integrations, which have to be performed for the AI approach, always introduce some errors in the computations, while such integrations are not required for the GST model.

References

[1] A. J. Schriefl, G. Zeindlinger, D. M. Pierce, P. Regitnig, and G. A. Holzapfel. Determination of the layer-specific distributed collagen fiber orientations in human thoracic and abdominal aortas and common iliac arteries. *J. R. Soc. Interface*, 9:1275–1286, 2012.

[2] A. J. Schriefl, H. Wolinski, P. Regitnig, S. D. Kohlwein, and G. A. Holzapfel. An automated approach for 3D quantification of fibrillar structures in optically cleared soft biological tissues. *J. R. Soc. Interface*, 10:20120760, 2013.

[3] G. A. Ateshian, V. Rajan, N. O. Chahine, C. E. Canal, and C. T. Hung. Modeling the matrix of articular cartilage using a continuous fiber angular distribution predicts many observed phenomena. *J. Biomech. Eng.*, 131:61003, 2009.

[4] M. B. Lilledahl, D. M. Pierce, T. Ricken, G. A. Holzapfel, and C. de Lange Davies. Structural analysis of articular cartilage using multiphoton microscopy: input for biomechanical modeling. *IEEE Trans. Med. Imaging*, 30:1635–1648, 2011.

[5] J. A. Niestrawska, Ch. Viertler, P. Regitnig, T. U. Cohnert, G. Sommer, and G. A. Holzapfel. Microstructure and mechanics of healthy and aneurysmatic abdominal aortas: experimental analysis and modeling. *J. R. Soc. Interface*, 13:20160620, 2016.

[6] W. J. Karlon, J. W. Covell, A. D. McCulloch, J. J. Hunter, and J. H. Omens. Automated measurement of myofiber disarray in transgenic mice with ventricular expression of ras. *Anat. Rec.*, 252:612–625, 1998.

[7] J. W. Covell. Tissue structure and ventricular wall mechanics. *Circulation*, 118:699–701, 2008.

[8] K. M. Meek, T. Blamires, G. F. Elliott, T. J. Gyi, and C. Nave. The organisation of collagen fibrils in the human corneal stroma: a synchrotron X-ray diffraction study. *CER*, 6:841–846, 1987.

[9] D. M. Pierce, W. Trobin, J. G. Raya, S. Trattnig, H. Bischof, Ch. Glaser, and G. A. Holzapfel. DT-MRI based computation of collagen fiber deformation in human articular cartilage: a feasibility study. *Ann. Biomed. Eng.*, 38:2447–2463, 2010.

[10] T. C. Gasser, R. W. Ogden, and G. A. Holzapfel. Hyperelastic modelling of arterial layers with distributed collagen fibre orientations. *J. R. Soc. Interface*, 3:15–35, 2006.

[11] G. A. Holzapfel, J. A. Niestrawska, R. W. Ogden, A. J. Reinisch, and A. J. Schriefl. Modelling non-symmetric collagen fibre dispersion in arterial walls. *J. R. Soc. Interface*, 12:20150188, 2015.

[12] T. S. E. Eriksson, A. J. Prassl, G. Plank, and G. A. Holzapfel. Modeling the dispersion in electro-mechanically coupled myocardium. *Int. J. Numer. Method Biomed. Eng.*, 29: 1267–1284, 2013.

[13] A. D. Freed, D. R. Einstein, and I. Vesely. Invariant formulation for dispersed transverse isotropy in aortic heart valves: An efficient means for modeling fiber splay. *Biomech. Model. Mechanobiol.*, 4:100–117, 2005.

[14] A. Pandolfi and G. A. Holzapfel. Three-dimensional modeling and computational analysis of the human cornea considering distributed collagen fibril orientations. *J. Biomech. Eng.*, 130:061006 (12 pages), 2008.

[15] Y. Lanir. Constitutive equations for fibrous connective tissues. *J. Biomech.*, 16:1–12, 1983.

[16] G. A. Holzapfel and R. W. Ogden. On the tension–compression switch in soft fibrous solids. *Eur. J. Mech. A/Solids*, 49:561–569, 2015.

[17] G. A. Holzapfel and R. W. Ogden. On fiber dispersion models: exclusion of compressed fibers and spurious model comparisons. *J. Elasticity*. in press. DOI:10.1007/s10659-016-9605-2

[18] K. Li, R. W. Ogden, and G. A. Holzapfel. Computational method for excluding fibers under compression in modeling soft fibrous solids. *Eur. J. Mech. A/Solids*, 57:178–193, 2016.

[19] K. Li, R. W. Ogden, and G. A. Holzapfel. An exponential constitutive model excluding fibers under compression: application to extension–inflation of a residually stressed carotid artery. *Math. Mech. Solids*. in press. DOI:10.1177/1081286517712077

[20] S. Federico and W. Herzog. Towards an analytical model of soft biological tissues. *J. Biomech.*, 41:3309–3313, 2008.

[21] D. H. Cortes, S. P. Lake, J. A. Kadlowec, L. J. Soslowsky, and D. M. Elliot. Characterizing the mechanical contribution of fiber angular distribution in connective tissue: comparison of two modeling approaches. *Biomech. Model. Mechanobiol.*, 9:651–658, 2010.

[22] A. Pandolfi and M. Vasta. Fiber distributed hyperelastic modeling of biological tissues. *Mech. Mat.*, 44:151–162, 2012.

[23] Y. Lanir and R. Namani. Reliability of structure tensors in representing soft tissues structure. *J. Mech. Behav. Biomed. Mater.*, 46:222–228, 2015.

[24] L. Ge. A characteristic-based constitutive law for dispersed fibers. *J. Biomech. Eng.*, 138: 071006–1–071006–8, 2016.

[25] R. W. Ogden. *Non-linear Elastic Deformations*. Dover, New York, 1997.

[26] G. A. Holzapfel. *Nonlinear Solid Mechanics. A Continuum Approach for Engineering*. John Wiley & Sons, Chichester, 2000.

[27] G. A. Holzapfel and R. W. Ogden. Constitutive modelling of arteries. *Proc. R. Soc. Lond. A*, 466:1551–1597, 2010.

[28] R. W. Ogden. Nonlinear continuum mechanics and modelling the elasticity of soft biological tissues with a focus on artery walls. In G. A. Holzapfel and R. W. Ogden, editors, *Lecture notes from the Summer School "Biomechanics: Trends in Modeling and Simulation" in Graz, Austria, in September, 2014*, Heidelberg, 2016. Springer.

[29] *Wolfram Research, Inc. Mathematica, Version 10.4.* Champaign, Illinois, 2016.

[30] M. S. Sacks. Incorporation of experimentally-derived fiber orientation into a structural constitutive model for planar collagenous tissues. *J. Biomech. Eng.*, 125:280–287, 2003.

Highlights

- Comparison of the predictions of the AI and GST fiber dispersion models for soft biological tissues

- It is shown that the predictions of the two models are virtually identical for a significant range of large deformations, contrary to claims in the literature

- Each of the models is fitted to sets of uniaxial data from the circumferential and axial directions of the adventitia of a human aorta, with both models providing excellent agreement with the data